

Film growth of BaZrO₃-doped YBa₂Cu₃O_{7-δ} by using fluorine-free metal-organic deposition

This article has been downloaded from IOPscience. Please scroll down to see the full text article.

2012 Supercond. Sci. Technol. 25 015011

(<http://iopscience.iop.org/0953-2048/25/1/015011>)

View [the table of contents for this issue](#), or go to the [journal homepage](#) for more

Download details:

IP Address: 146.201.213.155

The article was downloaded on 06/02/2012 at 15:44

Please note that [terms and conditions apply](#).

Film growth of BaZrO₃-doped YBa₂Cu₃O_{7- δ} by using fluorine-free metal–organic deposition

F Lu¹, F Kametani and E E Hellstrom

Applied Superconductivity Center, National High Magnetic Field Laboratory, Florida State University, Tallahassee, FL 32310, USA

E-mail: fenglu@physics.tamu.edu

Received 19 July 2011, in final form 4 October 2011

Published 6 December 2011

Online at stacks.iop.org/SUST/25/015011

Abstract

In this study, BaZrO₃ (BZO)-doped YBCO films were fabricated on SrTiO₃(100) single-crystal substrates by a fluorine-free metal–organic deposition (MOD) process. We added extra Ba and Zr organic salts, which formed well-dispersed ~10–25 nm sized BaZrO₃ nanoparticles in the YBCO films. The in-field critical current density (J_c) and the peak pinning force (F_p) were greatly enhanced in the BZO-doped sample at 77 K relative to pure YBCO films. The optimal BZO content that gave the highest peak pinning force of ~10 GN m⁻³ in a ~180 nm thick film was found to be $x = 0.10$ for YBCO + x BZO films, where x is moles of BZO per 1 mol of YBCO. The angular dependence of in-field J_c measurements shows the BZO nanoparticles increased J_c over the entire angular range and also reduced the angular anisotropy measured at 4 T at 77 K.

(Some figures may appear in colour only in the online journal)

1. Introduction

Many technological applications of high- T_c superconductors (HTS) require high critical current densities (J_c) in a magnetic field at 77 K. YBa₂Cu₃O_{7- δ} (YBCO) coated conductors made on rolling-assisted biaxially textured substrates (RABiTS) and on ion-beam-assisted deposition (IBAD) substrates can be used for these applications [1]. The in-field performance of YBCO can be enhanced by incorporating nanoparticles of RE₂O₃ (RE = rare earth) and/or nanoparticles or nanorods of BaZrO₃ (BZO) in the YBCO matrix [2, 3]. BZO nanorods can be grown by pulsed laser deposition (PLD) and metal–organic chemical vapor deposition (MOCVD) of YBCO + BZO films [4–6]. These are *in situ* processes in which the YBCO and BZO nucleate and grow during the deposition process. Depending on the deposition conditions, PLD and MOCVD can also grow BZO nanoparticles. In contrast only nanoparticles can be grown using *ex situ*

growth processes, such as the trifluoroacetate metal–organic deposition (TFA-MOD) process, where the precursor film containing the cations needed to form the film is deposited at room temperature then converted to YBCO + BZO by subsequent heating [7–9].

In this study we aimed to deposit high J_c YBCO films on single-crystal SrTiO₃ (STO) substrates using an *ex situ* fluorine-free MOD process and to enhance its in-field performance by adding BZO. The F-free MOD does not use F and thus simplifies the fabrication by avoiding the processing and safety issues associated with F and the HF gas that always evolves as YBCO forms in TFA-MOD. Yet it is applicable on as many templates or substrates as other YBCO film deposition techniques are, potentially being an alternative for scaling up to low-cost, long-length coated conductors on RABiTS or IBAD substrates. We made our precursor solutions drawing heavily on the F-free acetylacetonate-based MOD technique developed at the National Institute of Advanced Industrial Science and Technology (AIST) in Japan [10–13]. We investigated introducing BZO nanoparticles with the F-free

¹ Present address: Department of Physics and Astronomy, Texas A&M University, College Station, TX 77843, USA.

process because it has been reported [8] that a very high peak flux pinning force (F_p) $\sim 20 \text{ GN m}^{-3}$ at 77 K, $H \parallel c$ was attained by introducing BZO nanoparticles in TFA-MOD YBCO films.

2. Experimental details

The F-free precursor solutions were prepared by dissolving Y-, Ba-, and Cu-acetylacetonates (hereafter AcAc) (Alfa Aesar) in a 1:2:3 Y:Ba:Cu mole ratio in a mixture of pyridine (PY) and propionic acid (PA) (PY:PA=5:3 by volume) at room temperature. BZO-doped YBCO was made by adding Zr-AcAc and extra Ba-AcAc in a 1:1 Ba:Zr mole ratio to achieve an overall stoichiometry of the film given by $1\text{YBCO} + x\text{BZO}$, where x is the moles of BZO per 1 mol of YBCO. Films with $x = 0\text{--}0.15$ were synthesized. The exact degree of hydration of each AcAc was measured by heating a small sample of each AcAc in flowing air in a combination thermogravimetric plus differential thermal analysis system (TGA/DTA, TA Instruments 2960 SDT).

After the AcAc's were dissolved, the solution was heated to 70–80 °C in air to evaporate most of the solvents. This yielded a black, tar-like residue that was subsequently dissolved into methanol, forming a homogeneous dark-green solution. The total metal cation concentration in this final solution was adjusted to be $\sim 1 \text{ M}$.

The precursor films were prepared by depositing the final precursor solution on $10 \times 10 \text{ mm}^2$ (001)-oriented STO substrates (MTI Corp.) by spin-coating. The precursor solution was dropped onto the STO using a syringe. The STO was spun at $\sim 4000 \text{ rpm}$ for 30 s. The precursor films were converted to superconducting films in three steps. First the precursor films were heated in Ar to decompose the organic salts. DTA and TGA were used to understand the decomposition of the precursor film so as to design the decomposition heat treatment schedule. Details of this decomposition step are given in section 3.1. These decomposed films were directly inserted into a preheated tube furnace at 795 °C for 60 min in a flowing Ar atmosphere containing $150 \pm 50 \text{ ppm}$ oxygen. In the final step, the films were cooled down to 500 °C at $25 \text{ }^\circ\text{C min}^{-1}$ and held at 500 °C in 1 bar flowing oxygen for 2 h, then cooled to room temperature at $5 \text{ }^\circ\text{C min}^{-1}$. The final overall thickness of the films was $\sim 250\text{--}300 \text{ nm}$.

The surface and cross-sectional morphology of the films was investigated using a Carl Zeiss 1540EsB/XB Field Emission SEM with a focused ion beam (FIB). A transmission electron microscope (TEM) study was carried out using a JEOL JEM2011 microscope. X-ray diffraction (XRD) data were obtained using a PANalytical X'Pert diffractometer (Cu $K\alpha$). The sample resistance and critical current (I_c) were measured with a four-point configuration at 77 K in magnetic fields up to 9 T with the field perpendicular to the film surface ($H \parallel c$; 9 T Quantum Design Physical Property Measurement System (PPMS)). We cut a bridge $\sim 120 \text{ }\mu\text{m}$ wide and $\sim 500 \text{ }\mu\text{m}$ long in the film using an Nd:YAG laser (Amoco Laser Co.) to restrict I_c to $< 3 \text{ A}$ to prevent the sample from overheating. I_c was determined at an electric field

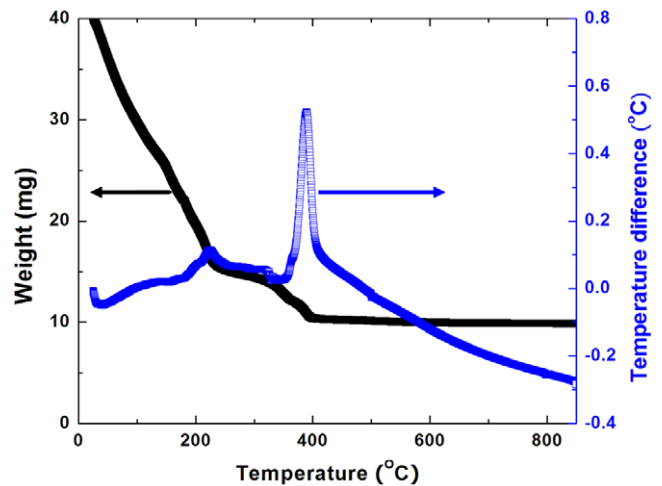


Figure 1. TGA and DTA plots of the 1 YBCO + 0.05 BZO precursor solution. The total metal cation concentration is 1.0 M. Heating ramp: $5 \text{ }^\circ\text{C min}^{-1}$ in Ar.

criterion of $1 \text{ }\mu\text{V cm}^{-1}$. Angular-dependent J_c measurements were performed by rotating the magnetic field relative to the plane of the film with the field always normal to the current.

3. Results

3.1. Decomposition of the precursor

Initially we decomposed the precursor film by heating it at $10 \text{ }^\circ\text{C min}^{-1}$ to 500 °C, holding it for 20 min, then cooling it to room temperature [10, 11]. However, this resulted in wrinkled films on STO substrates. The DTA/TGA study on the precursor material shown in figure 1 was done to understand where the AcAc's decompose to be able to design a heat treatment to prevent this wrinkling. The data in figure 1 show two distinct exothermic peaks in the DTA curve, one at $\sim 210 \text{ }^\circ\text{C}$ and a much bigger peak at $\sim 400 \text{ }^\circ\text{C}$. There are discrete changes in slope of the mass–temperature data corresponding to these thermal peaks. This observation is consistent with the individual decompositions of Y-AcAc, Ba-AcAc and Cu-AcAc. The continuous decrease in mass up to $\sim 230 \text{ }^\circ\text{C}$ is due to continuous loss of the organic solvents, whereas the first exothermic peak at $\sim 230 \text{ }^\circ\text{C}$ is due to the decomposition of Cu-AcAc and the first of two decomposition steps on Ba-AcAc. The second exothermic peak at $\sim 400 \text{ }^\circ\text{C}$ corresponds with the decomposition of Y-AcAc and the second decomposition step of Ba-AcAc. The constant mass above $\sim 410 \text{ }^\circ\text{C}$ corresponds to loss of all the organic solvents and all the AcAc's being decomposed.

The data in figure 1 were used to develop the two-plateau decomposition heating schedule in figure 2. The temperatures of the two plateaus were chosen based on the weight change and thermal peaks in figure 1. This decomposition schedule was used for pure and BZO-doped YBCO films. The two-plateau decomposition schedule improved the surface smoothness probably by providing a long time to remove the gases that are released when the AcAc's decompose.

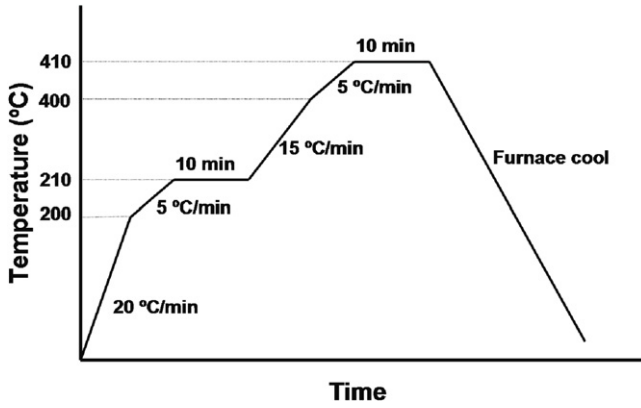


Figure 2. Two-plateau pyrolysis heat treatment in Ar.

Figure 3(a) shows a wrinkled film ($x = 0.10$) which was decomposed with one-step continuous heating to 500°C on STO, whereas figure 3(b) shows an $x = 0.10$ film that was decomposed using the two-plateau schedule, which has a homogeneous, pore-free, smooth surface. It also shows a few particles, identified as Cu–O and Ba–Cu–O phases by energy-dispersive x-ray spectroscopy (EDS), which are uniformly distributed on the surface.

3.2. Microstructure of fully processed films

Figure 4(a) is a cross-sectional image of a fully processed $x = 0.10$ film on STO, where the FIB was used to make the cut in the film. The image shows the film is dense and homogeneous with only a few pores present near the YBCO surface. Also, there are very few secondary phases present in the film. Figure 4(b) is a TEM cross-sectional image of the film in figure 4(a). It shows 10–25 nm diameter, approximately spherical, dark particles that were identified as BZO by indexing their TEM diffraction patterns. The BZO are well dispersed in the lateral direction parallel to the STO substrate. The image shows what appears to be a higher density of BZO particles close to the top of the film. This apparent difference in density is not real and is caused by the variation in thickness of the TEM specimen from milling, with the foil being thinner near the substrate. Figure 4(c) shows an XRD θ – 2θ pattern for the same film. There are two strong peaks from YBCO (004) and (005) and two minor but broad peaks from BZO (110) and (200). This is direct evidence that BZO particles formed during the growth of the YBCO film. The relatively weak intensity of the BZO peaks is due to the small volume fraction of BZO, small BZO particle size and almost random BZO orientation.

3.3. Electromagnetic properties

Table 1 lists electromagnetic data for the films made in this study. The T_c values for the films range from 90.8 K for pure YBCO to 86.2 K for the $x = 0.15$ film. Figure 5(a) displays J_c as a function of applied magnetic field H , for fully processed pure and BZO-doped films. The films with $x = 0.00$ – 0.10 have self-field J_c ranging from 2.4 to 2.8 MA cm^{–2} at 77 K,

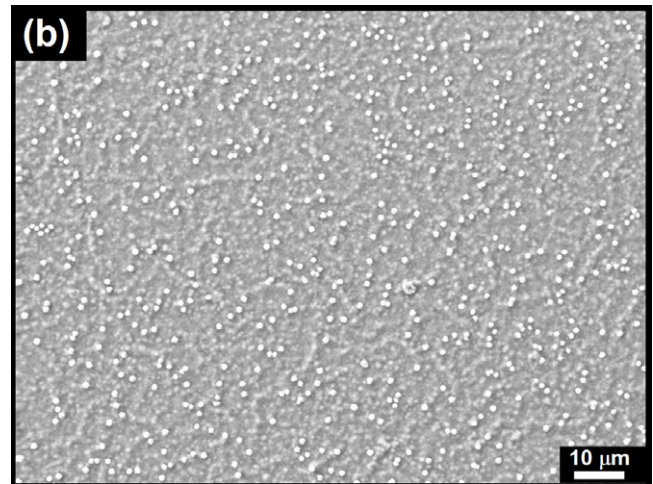
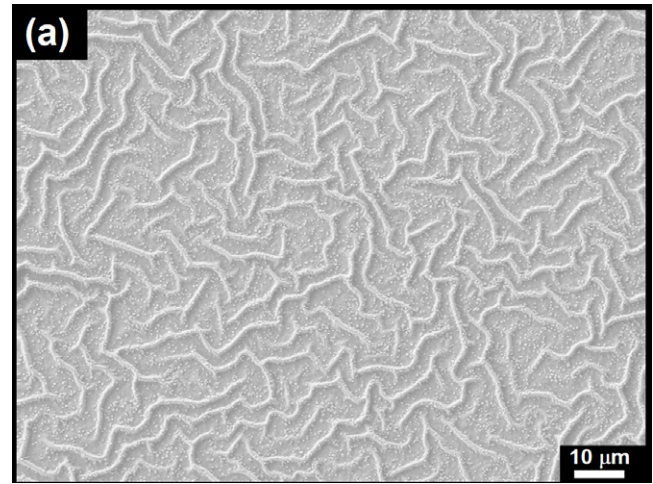


Figure 3. SEM image of a pyrolyzed YBCO + 0.10 BZO film on STO after (a) one-step and (b) two-plateau pyrolysis processes.

Table 1. Summary of T_c , and 77 K J_c (SF), F_p^{max} and H^{irr} for pure and BZO-doped YBCO films.

Content of BZO						
x	Mol%	Vol%	T_c (K)	J_c (SF, $H \parallel c$) (MA cm ^{–2})	Maximum F_p (GN m ^{–3})	H^{irr} (T)
0	—	—	90.8	2.59	1.7	6.3
0.05	4.76	2.35	89.0	2.36	5.9	8.0
0.10	9.09	4.60	88.1	2.78	9.8	8.5
0.15	13.04	6.73	86.2	1.35	2.3	6.4

$H \parallel c$, whereas J_c drops to 1.35 MA cm^{–2} for $x = 0.15$. J_c in the BZO-doped films decreases slower with increasing field than in the pure YBCO film. The film with $x = 0.10$ has the highest J_c in all fields. The irreversibility field H^{irr} of the films, determined using the 100 A cm^{–2} criterion, increased from ~6.2 T for pure YBCO to ~8 and 8.5 T for the $x = 0.05$ and 0.10 films, respectively.

The volume pinning force F_p , ($F_p = J_c \times H$), is shown in figure 5(b). The maximum F_p is for the $x = 0.10$ film, which has a maximum pinning force of ~10 GN m^{–3} at 77 K, $H \parallel c$, which is ~5 times greater than for pure YBCO films. In addition to increasing F_p , BZO doping also shifted the broad

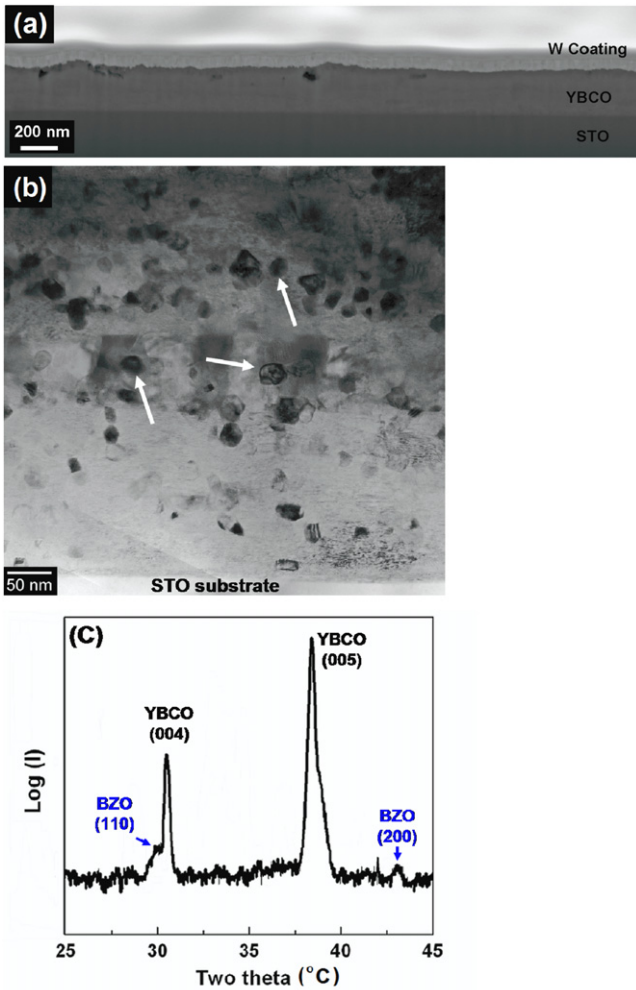


Figure 4. (a) FIB-SEM cross-sectional image, (b) TEM cross-section diffraction contrast image showing several BZO nanoparticles, which are indicated by white arrows and (c) XRD θ - 2θ pattern of a fully processed YBCO + 0.10 BZO film on STO.

maximum peak in the F_p - H plot from ~ 1 T for pure YBCO to ~ 1.75 T for the $x = 0.10$ film.

4. Discussion

The TFA-MOD process was developed so that BaF_2 rather than BaCO_3 forms when CO_2 is released as the organometallic TFA precursors decompose during heating [14]. In the TFA-MOD process, H_2O is used to convert BaF_2 to BaO releasing HF gas. We know from the work of Manabe *et al* [12, 13] that it is not a problem having BaCO_3 present as an intermediate phase when forming YBCO films with the F-free MOD process. X-ray diffraction patterns of our fully processed films, figure 4(c), did not show any peaks for BaCO_3 . In addition, the MOCVD process is also an F-free process, and there are no problems with residual BaCO_3 in the fully processed films [15]. Vermeir *et al* [16] comprehensively studied the YBCO reaction mechanism for aqueous F-free approaches. They reported that the presence of BaCO_3 is not fatal when forming YBCO, but rather

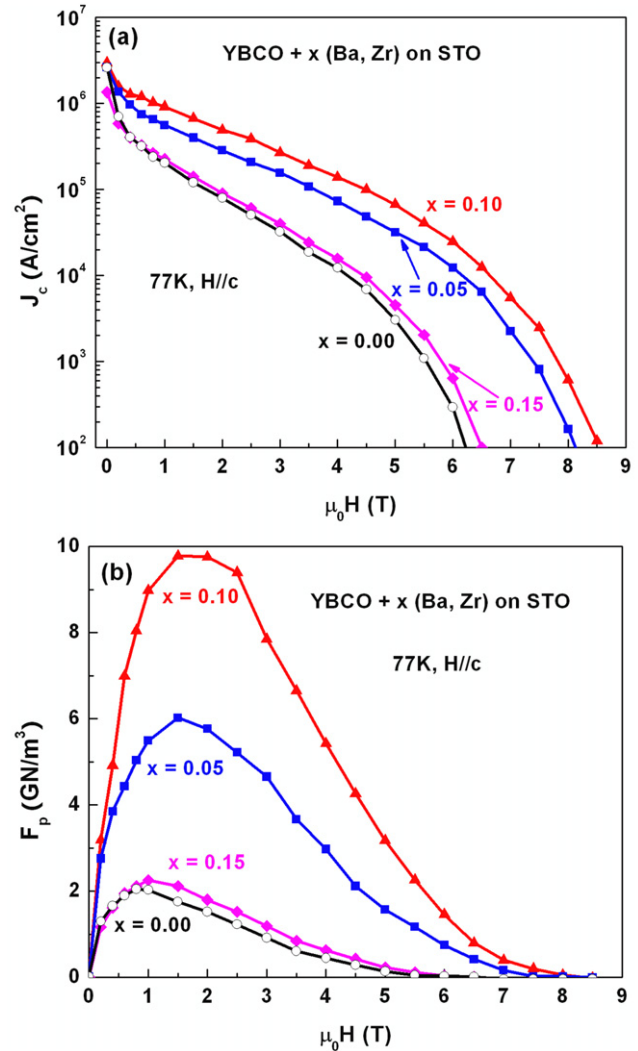


Figure 5. (a) J_c - H and (b) F_p - H at 77 K, $H \parallel c$, for YBCO + x BZO ($x = 0.00, 0.05, 0.10$ and 0.15) films on STO.

it is a desired intermediate phase when synthesizing bulk or thin-film YBCO. They reported that BaCO_3 and CuO react forming BaCuO_2 first and this BaCuO_2 reacts with the remaining CuO forming a eutectic liquid that reacts with Y_2O_3 to form YBCO. They confirmed this mechanism using high-temperature XRD experiments. Even though we used organic solvents in our study rather than aqueous solutions, we speculate that YBCO forms by a similar reaction mechanism in our F-free MOD films.

Modifying the decomposition procedure (figure 2) for the precursor film was important to improve the overall film quality as seen in figure 3.

At 77 K, the self-field J_c of the pure YBCO film reaches 2.6 MA cm^{-2} , with $T_c \sim 91$ K and $H^{irr} \sim 6.3$ T. These relatively high values are comparable to those in TFA-MOD YBCO films and in films made with an F-free MOD on CeO_2 -buffered single-crystal sapphire [12].

The BZO nanoparticles were successfully formed in the F-free MOD films. They increase the pinning force measured at 77 K self-field, even though BZO addition decreased T_c (see table 1), which has been reported for BZO-doped YBCO

films [4, 5] deposited by PLD. The reason for T_c degradation with BZO-doping in F-free MOD YBCO is not clear yet. Nevertheless, it is particularly interesting that J_c (77 K, SF) remains almost unchanged, ranging from 2.4 to 2.8 MA cm⁻² (77 K, SF), as T_c in the film decreases with increasing BZO content (table 1).

The maximum peak pinning force of ~ 10 GN m⁻³ at 77 K, $H \parallel c$ is for the $x = 0.10$ film. This is smaller than the value of ~ 20 GN m⁻³ Gutierrez *et al* [8] reported for a 10 mol% BZO-doped TFA-MOD YBCO film grown on single-crystal STO substrates. We do not know why our peak F_p is about half that reported by Gutierrez *et al* [8] even though the BZO nanoparticles in our film look very similar to those reported in [8, 9]. It is worth noting that T_c in their TFA-MOD film [8] was 91 K, which is significantly higher than most BZO-doped YBCO films and is 3 K higher than in our $x = 0.10$ film. The maximum of the broad peak in the F_p - H plot shifts from ~ 1 T for pure YBCO to ~ 1.75 T for the $x = 0.10$ film. This shift is the same as seen for BZO-doped TFA-MOD films on CeO₂ buffered IBAD [7] and single-crystal STO [8] substrates. For YBCO films grown on IBAD templates, Miura *et al* [7] achieved J_c of 3.7 MA cm⁻² and F_p^{\max} of ~ 7.5 GN m⁻³ at around 1.5–2 T for 1 μ m thick 1 wt% BZO-doped YBCO films grown by TFA-MOD on ion-beam-assisted deposition (IBAD) substrates. Strickland *et al* [9] fabricated ~ 800 nm thick 10 mol% BZO-doped YBCO films on biaxially textured substrates (RABiTS) using TFA-MOD and achieved I_c of 200–245 A cm⁻¹ width (equal to 2.5–3.0 MA cm⁻²) and $F_p^{\max} \sim 5$ GN m⁻³ at around 1.5–2 T.

The BZO nanoparticles in figure 4(b) are roughly spherical in shape and are uniformly distributed in the film. They are 10–25 nm in diameter, which is slightly larger than the ideal size to pin flux, which is 2ξ , where $\xi = 4$ nm is the coherence length of YBCO at 77 K [17]. The peak pinning force, ~ 10 GN m⁻³, for the $x = 0.10$ film shows adding BZO nanoparticles effectively improves the pinning force in our YBCO films. Gutierrez *et al* reported the coexistence of epitaxial and randomly oriented BZO particles, roughly in the ratio of 1:9 for a 10 mol% BZO sample, and pointed out that the origin of isotropic pinning in BZO-doped YBCO films is not the nanoparticles themselves, but the nanostrain created in the matrix around them [8]. However, there are also reports [6, 7, 9, 18] ascribing the pinning enhancement to the homogeneously dispersed BZO (and/or RE₂O₃) nanoparticles, which had similar sizes to the BZO pins we see in our film, acting as effective pins for magnetic flux. High resolution TEM studies, which we have not done, would be needed to study the interface between our BZO nanoparticles and YBCO to distinguish the pinning mechanism.

Evidence of reduced anisotropy by BZO doping comes from the angular dependences of J_c . Figure 6 shows $J_c(\theta)$ plots for pure and $x = 0.10$ films at an applied field of 4 T. In addition to a general increase in J_c for the $x = 0.10$ film over the whole angular range, doping with BZO also decreases the J_c anisotropy. The ratio of $J_c(H \parallel ab):J_c(H \parallel c)$ was used to evaluate the anisotropy. At 4 T, this ratio decreased from ~ 16

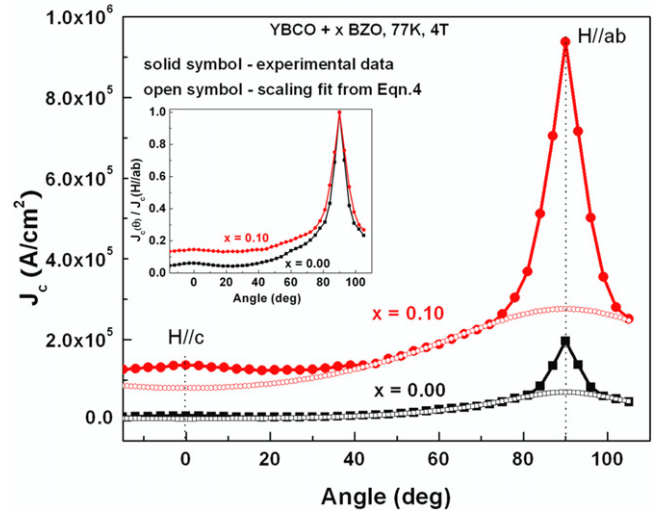


Figure 6. $J_c(\theta)$ at 77 K, 4 T for YBCO + x BZO ($x = 0.00$ and 0.10) films on STO and the fit using equation (4). $\gamma = 4$ for $x = 0.00$ and $\gamma = 2$ for $x = 0.10$. The inset shows $J_c(\theta)$ normalized to $J_c(H \parallel ab)$.

for pure YBCO to ~ 7 for $x = 0.10$, which is shown in the inset in figure 6.

To understand flux pinning, Kramer proposed that F_p in Nb superconductors follows the scaling rule [19]:

$$F_p = K_p h^{1/2} (1 - h)^2 \quad (1)$$

where K_p is a constant, and h the reduced field $h = H/H_{irr}$. For HTS films, equation (1) can be rewritten by replacing $1/2$ with α , and 2 with β . So we have

$$F_p = K_p h^\alpha (1 - h)^\beta \quad (2)$$

Since $F_p = J_c \times B$, we can describe J_c (when $H \neq 0$) by

$$J_c = A h^{\alpha'} (1 - h)^{\beta'} \quad (3)$$

We then rewrite α' as α and β' as β for simplification. The exponents α and β for the two samples in this study are determined by fitting the experimental $J_c(H)$ data in the $H \parallel c$ direction to equation (3). In this way, α and β are found to be -0.55 and 2.44 for the pure YBCO sample, and -0.2 and 2.99 for the BZO-doped sample, respectively.

Now we can add in Blatter's angular scaling approach which allows us to calculate the angular dependence of $J_c(\theta, H)$ from the field dependence of $J_c(H)$ for $H \parallel c$, by rescaling the applied field according to $H \rightarrow Hf(\theta)$, where $f(\theta) = (\cos^2\theta + (1/\gamma)^2 \sin^2\theta)^{1/2}$, θ is the angle between H and the c axis, and γ is the electron mass anisotropy factor. Then the general dependence of $J_c(\theta, H)$ can be presented in the following generic scaling form [20]:

$$J_c(\theta, H) = J_0 \left(\frac{Hf(\theta)}{H_{irr}} \right)^\alpha \left(1 - \frac{Hf(\theta)}{H_{irr}} \right)^\beta \quad (4)$$

The experimental $J_c(\theta, 4$ T) data for the pure YBCO sample were fitted by equation (4) using $\gamma = 4$, as shown in figure 6. Equation (4) does not fit the peaks in J_c seen

around $H \parallel ab$ and $H \parallel c$. The relatively large peak centered at $H \parallel ab$ is generally caused by intrinsic pinning centers as a consequence of the layered crystallographic structure and other correlated structures parallel to the ab planes [7, 21]. The small peak centered at $H \parallel c$, is due to the correlated disorder along the c axis, which is not as big in the MOD films as in PLD films that have lots of defects along the c axis such as twin boundaries, stacking faults and dislocations arising mainly from the columnar grain structure [21, 22].

For the $x = 0.10$ film, the data were fitted with $\gamma = 2$, as shown in figure 6. The smaller γ for the $x = 0.10$ film indicates adding BZO nanoparticles reduced the intrinsic anisotropy of MOD YBCO films, which have $\gamma \sim 5-7$ [23] for pure YBCO. The inset in figure 6 is $J_c(\theta)$ normalized to $J_c(H \parallel ab)$, which clearly shows the reduced anisotropy. Again equation (4) does not fit the peaks centered at $H \parallel ab$ and $H \parallel c$. In our films, the uniformly distributed spherical BZO nanoparticles enhance the pinning in all directions, which is responsible for the overall increase in J_c over the entire angular range compared to pure YBCO and for the increased F_p^{\max} . The peak at $H \parallel c$ in our $x = 0.10$ film is small and broad. This is in contrast to *in situ* films that have BZO nanorods that form parallel to the c -axis growth direction and characteristically have a strong peak centered at $H \parallel c$ due to strong pinning of the flux lines when they are parallel to the nanorods [4, 5].

5. Conclusion

We incorporated BZO nanoparticles in YBCO films by adding extra Ba and Zr organometallic salts to the F-free YBCO precursor solution. The BZO, which formed during the *ex situ* reaction, were spherical, 10–25 nm in diameter, randomly oriented, and uniformly distributed in the YBCO. Their presence increased the in-field $J_c(\theta)$ at all angles and also increased the flux pinning. The $x = 0.10$ film exhibited the highest pinning force of $\sim 10 \text{ GN m}^{-3}$. The BZO-doped films also exhibited a reduced J_c anisotropy, making them attractive for practical applications in fields at 77 K.

Acknowledgments

We are grateful for valuable discussions with David Larbalestier and Zhijun Chen. This work was supported by an US Air Force Office of Scientific Research (AFOSR) grant through the Multidisciplinary University Research Initiative

(MURI) and by the Department of Energy (DOE)—Office of Electricity Delivery and Energy Reliability (OEDER).

References

- [1] Larbalestier D C, Gurevich A, Feldmann D M and Polyanskii A 2001 *Nature* **414** 368–77
- [2] Macmanus-Driscoll J L, Foltyn S R, Jia Q X, Wang H, Serquis A, Civale L, Maiorov B, Hawley M E, Maley M P and Peterson D E 2004 *Nature Mater.* **3** 439–43
- [3] Haugan T, Barnes P N, Wheeler R, Meisenkothen F and Sumption M 2004 *Nature* **430** 867–70
- [4] Kang S et al 2006 *Science* **311** 1911–4
- [5] Mele P, Matsumoto K, Horide T, Ichinose A, Mukaida M, Yoshida Y, Horii S and Kita R 2008 *Supercond. Sci. Technol.* **21** 032002
- [6] Xu A, Jaroszynski J J, Kametani F, Chen Z, Larbalestier D C, Viouchkov Y L, Chen Y, Xie Y and Selvamanickam V 2010 *Supercond. Sci. Technol.* **23** 014003
- [7] Miura M, Kato T, Yoshizumi M, Yamada Y, Izumi T, Shiohara Y and Hirayama T 2008 *Appl. Phys. Express* **1** 051701
- [8] Gutierrez J et al 2007 *Nature Mater.* **6** 367–73
- [9] Strickland N M, Long N J, Talantsev E F, Hoefakker P, Xia J, Rupich M W, Kodenkandath T, Zhang W, Li X and Huang Y 2008 *Physica C* **468** 183–9
- [10] Kumagai T, Manabe T, Kondo W, Minamiue H and Mizuta S 1990 *Japan. J. Appl. Phys.* **29** L940–2
- [11] Manabe T, Kondo W, Mizuta S and Fumiga T 1994 *J. Mater. Res.* **9** 858–64
- [12] Manabe T, Sohma M, Yamaguchi I, Kondo W, Tsukada K, Mizuta S and Kumagai T 2004 *Physica C* **412–414** 896–9
- [13] Tsukada K, Yamaguchi I, Sohma M, Kondo W, Kamiya K, Kumagai T and Manabe T 2007 *Physica C* **458** 29–33
- [14] Gupta A, Jagannathan R, Cooper E I, Giess E A, Landman J I and Hussey B W 1988 *Appl. Phys. Lett.* **52** 2077–9
- [15] Hatzistergos M S, Efstathiadis H, Reeves J L, Selvamanickam V, Allen L P, Lifshin E and Haldar P 2004 *Physica C* **405** 179–86
- [16] Vermeir P, Cardinael I, Schaubroeck J, Verbeken K, Bäcker M, Lommens P, Knaepen W, D'haen J, Buysser K D and Driessche I V 2010 *Inorg. Chem.* **49** 4471–7
- [17] Gurevich A 2007 *Supercond. Sci. Technol.* **20** S128–35
- [18] Miura M, Bailly S A, Maiorov B, Civale L, Willis J O, Marken K, Izumi T, Tanabe K and Shiohara Y 2010 *Appl. Phys. Lett.* **96** 072506
- [19] Kramer E J 1972 *J. Appl. Phys.* **44** 1361
- [20] Chen Z, Feldmann D M, Song X, Kim S I, Gurevich A, Reeves J L, Xie Y Y, Selvamanickam V and Larbalestier D C 2007 *Supercond. Sci. Technol.* **20** S205–10
- [21] Civale L et al 2004 *Appl. Phys. Lett.* **84** 2121–3
- [22] Holesinger T G et al 2008 *Adv. Mater.* **20** 391–407
- [23] Puig T and Obradors X 2000 *Appl. Phys. Lett.* **84** 1571–4